Int. J. Heat Mass Transfer. Vol. 33, No. 8, pp. 1737–1749, 1990
Printed in Great Britain

0017-9310/90 $3.00 + 0.00

Prediction of film condensation on vertical finned plates and tubes: a model for the drainage channel

THOMAS ADAMEK
Universität Stuttgart, D-7000 Stuttgart, F.R.G.

and

RALPH L. WEBB
Department of Mechanical Engineering, The Pennsylvania State University, University Park, PA 16802, U.S.A.

(*Received* 6 *March* 1989 *and in final form* 23 *October* 1989)

Abstract—In 1954, Gregorig formulated a theory for surface tension drained condensation on vertical 'fluted' surfaces, which have a special convex fin profile. Typically, such fluted surfaces must also have a drainage channel, in which the condensate generated on the special convex profile is drained by gravity force. The literature has been devoid of a satisfactory model to predict the condensation rate in the drainage channel. This paper formulates a theoretical method to predict the condensation rate in a drainage channel of rectangular cross-section. The model was used to predict the experimental data of Kedzierski and Webb, and is shown to provide an excellent prediction of the data. The prediction shows that the condensation rate in the drainage channel accounted for 6–32% of the total condensation rate on the Gregorig convex fin profile, as tested by Kedzierski and Webb. With slight modification, the drainage channel model may be extended to predict the condensation rate in drainage channels having other than a rectangular shape, e.g. a cosine shape.

1. INTRODUCTION

THE EFFECT of surface tension force on film condensation was first discovered by Gregorig [1]. When condensation occurs on a vertical surface having convex fins, and concave drainage channels, surface tension force will pull the condensate from the convex profile (Fig. 1) into the concave drainage channels, which are gravity drained. Presently, most analytical models for prediction of the heat transfer rate typically ignore the condensation rate in the concave drainage channels. Typical of such models are Gregorig [1], Karkhu [2], Zener and Lavi [3], Webb [4], Fujii and Honda [5], Mori *et al.* [6], Panchal and Bell [7], and Adamek [8, 9]. Zener and Lavi [3] and Webb [4] defined the necessary width and depth of the drainage channel, but they ignored the condensation rate that occurs on the walls of the channel.

A closely related problem is that of condensation on horizontal, integral fin tubes. Typically, these tubes do not have the special profile shapes analyzed by Gregorig [1] or Adamek [8]. The integral fin tubes usually have fins of a trapezoidal or rectangular cross-sectional shape. However, Webb *et al.* [10] and Webb and Rudy [11] have shown that surface tension drains the fins. Webb and Rudy [11] and Honda and Nozu [12] developed theoretical models for condensation on such finned tubes. The Honda and Nozu model included a procedure to predict the condensation rate on the fin sides and in the base channel. The horizontal integral fin tube analysis must also account for condensate retention between the fins, on the lower side of the tube. This phenomenon is not involved in the vertical finned plate problem.

This paper is concerned with the vertical finned plates, and the condensation that occurs in the drainage channel. One may question the validity and completeness of theoretical models that ignore condensation in the drainge channel region. Hence, a key objective of this work is to define the condensation rate that actually occurs in the drainage channel. Figure 2 shows how the drainage channel fills along the condensing length. Figure 3 shows that the interface in the drainage channel has a concave circular shape. This will affect a surface tension force, which acts to pull condensate into the concave drainage channel. This action will establish the two additional thin film regions illustrated by line segments 2–3 and 4–5 in Fig. 1.

This study presents an analysis to calculate the condensation in the concave channel region. Unfortunately, very little data exist to validate the predictive model. However, the data of Kedzierski and Webb [13] are directly applicable, and will be used here. Much more data exist for condensation on horizontal, integral fin tubes. Adamek and Webb [14] show how the present analysis may be modified and applied to the horizontal integral fin tube problem.

NOMENCLATURE

A	area of cross-section of drainage with circular shape [m^2]
d_H	hydraulic diameter, $4A/P$
D	spacing between adjacent fins [m]
e	fin height [m]
f	fraction factor
F_p	property group, $4k\nu\Delta T/\lambda$ [kg m s^{-2}]
g	gravitational constant [m s^{-2}]
h	condensation coefficient [W m^{-2} K^{-1}]
H	height of lateral channel side [m]
k	thermal conductivity of condensate [W m^{-1} K^{-1}]
l_{ik}	length between points $x = i$ and k
L	plate length [m]
$\dot{m}_{ik}$	condensate (flow) rate on region L_{ik} [kg s^{-1} m^{-1}]
$\dot{M}$	drainage flow rate in z-direction [kg s^{-1}]
$\dot{M}_{ik}$	total condensate rate between points $x = i$ and k at the plate ($0 \leqslant z \leqslant L$) [kg s^{-1}]
$\dot{M}_{index}$	total condensation rate by the 'index' defined below [kg s^{-1}]
$\dot{M}_{plate}$	total condensate rate at plate [kg s^{-1}]
N	number of fins
P	wetted perimeter [m]
p	pressure difference compared to saturation pressure [N m^{-2}]
Q_{ik}	total heat load at plate on region L_{ik} [W]
Q_{index}	total heat load on area denoted by 'index' defined below [W]
R	radius of curvature of interface in the drainage area [m]
R^*	projected length of R to lateral fin wall [m]
r	local radius of film surface [m]
s	coordinate between l_i and l_k [m]
ΔT	temperature difference between film and wall [K]
u	film velocity in x-direction [m s^{-1}]
x	direction on fin surface from tip to base [m]
w	film velocity in z-direction [m s^{-1}]
z	direction of drainage flow at plate [m].

Greek symbols

α	angle in Figs. 3 and 4 [rad]
β	angle in Figs. 3 and 4 [rad]
δ	film thickness [m]
δ_{ik}	film thickness between points $x = i$ and k [m]
Δ	condensate film thickness in the channel [m]
η	dynamic viscosity of condensate [kg s^{-1} m^{-1}]
η_f	fin efficiency [dimensionless]
κ	curvature of interface [m^{-1}]
κ'	$d\kappa/ds$ [m^{-2}]
λ	latent heat of vaporization of condensate [W s kg^{-1}]
ν	kinematic viscosity of condensate [m^2 s^{-1}]
ξ	characteristic parameter of fluted fin shape
ρ	density of condensate [kg m^{-3}]
σ	surface tension of condensate [N m^{-1}]
τ_w	wall shear stress [N m^{-2}]
ω	characteristic parameter of fluted fin shape.

Indices

b	channel base
C	convex profile
Cha	channel
s	channel side wall
tot	total.

2. FILM FLOW ON A VERTICAL FINNED PLATE

Figure 1 shows the general characteristics of film flow on a vertical finned plate having a drainage channel of rectangular cross-section. Figure 2 shows the liquid–vapor interface shape of the film in the concave drainage channel at several positions along the length of the plate. Near the top of the plate (Fig. 2(a)), the film is very thin, and has a nearly uniform thickness. The radius of the interface increases along the plate length, until the two segments of the film join to form a smooth, circular interface, whose radius is approximately $R = D/2$, where D is the channel width (Fig. 2(d)). This will occur if the plate is sufficiently long to carry the amount of condensate needed for the smooth, circular arc to form. The thickness of the condensate at the base of the channel is Δ. The pressure difference in the film between the inflection point on the channel side wall and the center, base of the channel is given by the Laplace equation as $\Delta p = \sigma/R$. For axial positions between Figs. 2(d) and (f), the interface radius in the concave channel remains constant, and the liquid depth in the channel increases. At the axial position illustrated by Fig. 2(g), the radius of the film has reached the fin tips, and the condensate begins to spread at the top of the fins. Then, the interface radius will be greater than $D/2$.

3. CONDENSATE FILM VELOCITY IN THE DRAINAGE CHANNEL

Based on the average film velocity in the channel $w(z)$, the condensate mass flow rate is given by the continuity equation as

$$\dot{M}(z) = \rho w(z) A(z). \quad (1)$$

Gravity pulling downward is opposed by shear stress on the channel wall. This force balance shows that

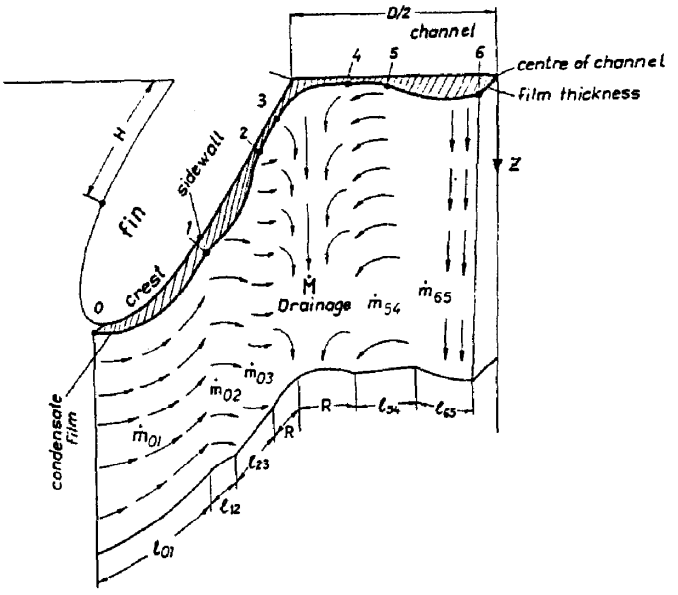

FIG. 1. Schematic of condensate flow on a vertical plate having surface tension drained fin profiles.

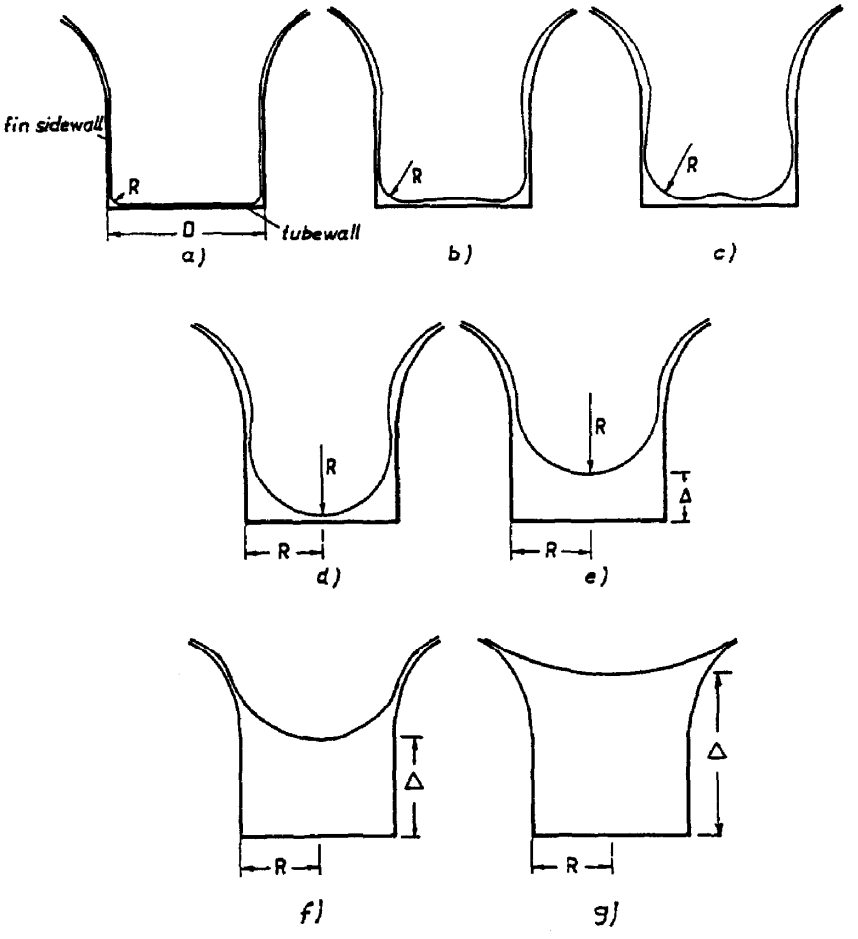

FIG. 2. Illustration showing how the radius in the drainage channel increases with plate length.

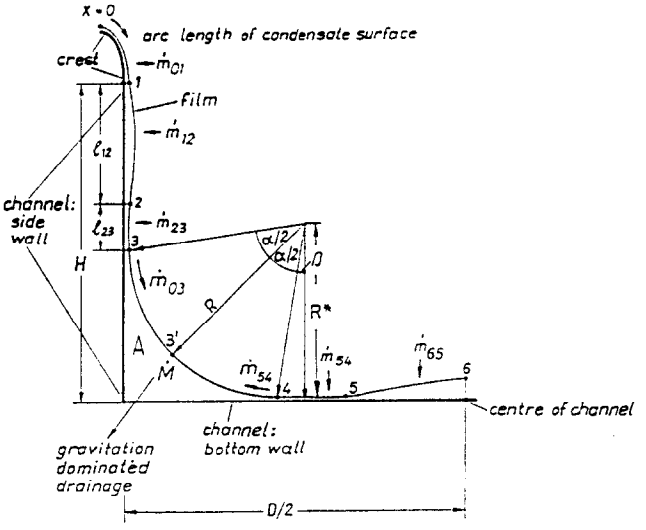

FIG. 3. Cross-section of fin and drainage channel cross-section, with definition of condensate drainage regions. Not to scale.

$$\tau_w = \tfrac{1}{2} f \rho w^2 = \frac{A}{P} \rho g \tag{2}$$

where $A = R^2 - \pi R^2/4 = 0.215R^2$, is the film cross-sectional area, and $P = 2R$ is the wall perimeter on which the shear stress, τ_w, acts.

Based on Thomas's analysis [15], the friction factor for laminar flow in a channel having a semi-circular interface is $12/Re$. This may be written as

$$f = \frac{12}{Re} = \frac{12\nu}{d_H w}. \tag{3}$$

Substitution of equation (3) in equation (2), and solving for w, gives

$$w = \frac{g d_H^2}{24\nu}. \tag{4}$$

Substitution of equation (4) in equation (1), writing A and P in terms of R, and using $d_H = 0.43R$ gives the mass flow rate in terms of the interface radius as

$$\dot{M}(z) = \frac{\rho g}{\nu} \frac{0.43^2 \times 0.215}{24} R^4(z) = 0.0017 \frac{\rho g}{\nu} R^4(z). \tag{5}$$

Equation (5) shows that the mass flow rate is related to the fourth power of R. If the channel cross-sectional shape is different than the rectangular one used here, a different equation would result for equation (5). However, the principles involved in the derivation of the equation would remain the same.

4. CONDENSATION IN THE DRAINAGE CHANNEL

4.1. *Basis of the analytical model*

At any axial position z on Fig. 1, the condensate rate carried by the channel results from the condensate formed on the convex profile, $\dot{M}_C$, and in the channel, $\dot{M}_{Cha}$. Thus

$$\dot{M}_{tot}(z) = \dot{M}_C(z) + \dot{M}_{Cha}(z). \tag{6}$$

Figure 3 shows a cross-section of the film at axial position z. This figure shows the condensate generated per unit z length, $\dot{m}$, in the separate regions to be modeled. The $\dot{m}_{01}$ is formed on the convex profile, and is independent of z. Hence, at any point z, $\dot{M}_{tot}$ is the sum of

$$\dot{M}_{tot}(z) = \dot{m}_{01} \cdot z + \int_0^z \dot{m}_{12}(t) + \dot{m}_{23}(t) + \dot{m}_{54}(t) + \dot{m}_{65}(t)\, dt \tag{7}$$

where $\dot{M}_C(z)$ and $\dot{M}_{Cha}(z)$ in equation (6) correspond to $\dot{m}_{01} \cdot z$, and the sum of the integrals in equation (7), respectively. Equation (7) assumes that the condensation rate in the thick film region 3–4 in Fig. 3 is negligible. The incremental length Δx for each region in the equation (7) integral is illustrated as the l_{ik} increments in Figs. 1 and 3. The integrated value over $0 < t < z$ for each of the integral terms in equation (7) is symbolically written as

$$\dot{M}_{ik}(z) = \int_0^z \dot{m}_{ik}(t)\, dt. \tag{8}$$

We will use the abbreviation $\dot{M}_{ik} = \dot{M}_{ik}(L)$, where L is the plate length. Our analysis will separately predict the condensation rates on the side and bottom of the drainage channel. Using the above terminology, the condensation on the side of the channel is

$$\dot{M}_{Sid} = \dot{M}_{13} = \dot{M}_{12} + \dot{M}_{23} = \int_0^L \dot{m}_{12}(z) + \dot{m}_{23}(z)\, dz. \tag{9}$$

In the same manner, the condensation rate on the bottom of the channel is

$$\dot{M}_{\mathrm{Bot}} = \dot{M}_{64} = \dot{M}_{65} + \dot{M}_{54} = \int_0^L \dot{m}_{65}(z) + \dot{m}_{54}(z)\,\mathrm{d}z. \tag{10}$$

Combining equations (6), (9) and (10), we get

$$\dot{M}_{\mathrm{tot}} = \dot{M}_{\mathrm{C}} + \dot{M}_{\mathrm{Cha}} = \dot{M}_{\mathrm{C}} + \dot{M}_{\mathrm{Sid}} + \dot{M}_{\mathrm{Bot}}. \tag{11}$$

4.2. *Condensation rate on the convex profile*

The condensation rate on the convex profile, l_{01}, depends on the shape of the convex profile. We will assume that the profile of interest and the governing theoretical equation have been separately specified. For example, Adamek [8] has defined a 'family' of convex profiles, whose condensation rate is given by

$$\dot{m}_{01} = 2.15\left(\left(\frac{k\Delta T}{\lambda}\right)^3\left(\frac{\rho\sigma}{\eta}\right)\omega\left(\frac{(\xi+1)}{(\xi+2)^3}\right)l_{01}\right)^{1/4} \tag{12}$$

where the profile shape is governed by the parameters ξ and ω.

4.3. *Calculation methodology for the drainage channel*

For gravity drained film condensation, Nusselt showed that $\alpha = k/\delta$. The film thickness, δ, is given by

$$\delta(x) = (F_{\mathrm{p}}x/\rho g)^{1/4}. \tag{13}$$

For the present problem, it is assumed that surface tension force dominates over gravity force. Hence, the gravity force per unit volume in equation (13) may be replaced by the surface tension induced pressure gradient

$$\mathrm{d}p/\mathrm{d}s = \sigma\cdot\mathrm{d}\kappa/\mathrm{d}s = \sigma\cdot\mathrm{d}(1/r)/\mathrm{d}s \tag{14}$$

where r is the local radius of the condensate interface. We will assume a linear pressure gradient in each of the incremental length regions. Hence, for a generalized region l_{ik}

$$\mathrm{d}p/\mathrm{d}s = \sigma(\kappa_k - \kappa_i)/l_{ik} = \sigma[(1/r_k) - (1/r_i)]/l_{ik} \tag{15}$$

where r_i and r_k are the local radii at the beginning and end of the length l_{ik}, respectively. The length over which equation (15) applies, l_{ik}, will replace x in equation (13). Hence, equation (13) may be adapted to calculate the condensation rate in each of the l_{ik} regions of Fig. 3, if $\mathrm{d}\kappa/\mathrm{d}s$ and l_{ik} can be defined for each of these regions.

4.4. *Condensation on the side wall*

4.4.1. *Definition of two regions.* The model must account for condensation on regions l_{12} and l_{23} shown in Fig. 3. Figure 4 shows that the curvature is small at x_1 and x_{21}, and that $\kappa(x_3) = 1/R$. Hence, the curvature change between points x_1 and x_2 should be quite small. Thus, the major curvature change occurs between points x_2 and x_3. So, the condensation rate should be substantially higher on region l_{23} than on region l_{12}. We shall derive an equation for the condensation rate on length l_{23}, and then approximate the condensation rate on length l_{12}, based on our knowledge of that occurring on l_{23}. Using the known values of $r_3 = R$ and $r_2 \simeq \infty$ in equation (15) gives

$$[\mathrm{d}p/\mathrm{d}s]_{23} = \sigma/Rl_{23}. \tag{16}$$

4.4.2. *Condensation on l_{23}.* It is now necessary to determine l_{23}. The total length of the drainage channel side wall, H, in Fig. 3 may be written as

$$H = l_{12} + l_{23} + R^* + \Delta \tag{17}$$

where R^* is the projection of R on the side wall. Note that the length of the convex profile is not included in the definition of H. Substitution of equation (5) in equation (7) and solving for the radius of the condensate film at the channel, $R(z)$, gives

$$R(z) = \left(\frac{\nu}{0.0017\rho g}\left(\dot{m}_{01}\cdot z + \int_0^z \dot{m}_{12}(z) + \dot{m}_{23}(z) + \dot{m}_{54}(z) + \dot{m}_{65}(z)\,\mathrm{d}z\right)\right)^{1/4}. \tag{18}$$

An approximate relation for $R(z)$ may be established by noting that the condensation rate on the convex profile, l_{01}, should be substantially higher than that in the drainage channel. Hence, we may simply neglect the condensation rate in the drainage channel for determination of $R(z)$. This is a reasonable approximation, since $R(z)$ depends on the 1/4 power of the condensation rate. For example, a 20% error in the condensation rate will result in an error of $R(z)$ of only 4.6%. The resulting approximation for $R(z)$ is

$$R(z) = \left(\frac{\nu}{0.0017\rho g}\dot{m}_{01}\cdot z\right)^{1/4}. \tag{19}$$

In the Appendix, we show that l_{23} and R^* may be expressed by equations (20) and (21)

$$l_{23}(z) \simeq l_{54}(z) = [F_{\mathrm{p}}R^5(z)/\sigma]^{1/6} \tag{20}$$

$$R^*(z) = R(z)\cos\left(\frac{l_{23}(z)}{2R(z)}\right). \tag{21}$$

Substituting equations (19) and (20) in the Nusselt equation (equation (13)), along with use of equation (16), the Appendix shows that

$$\delta_{23}(s) = \left(\left(\frac{3\nu\dot{m}_{02}l_{23}R}{\sigma}\right)^{4/3} + F_{\mathrm{p}}\left(\frac{l_{23}R}{\sigma}\right)s\right)^{1/4}. \tag{22}$$

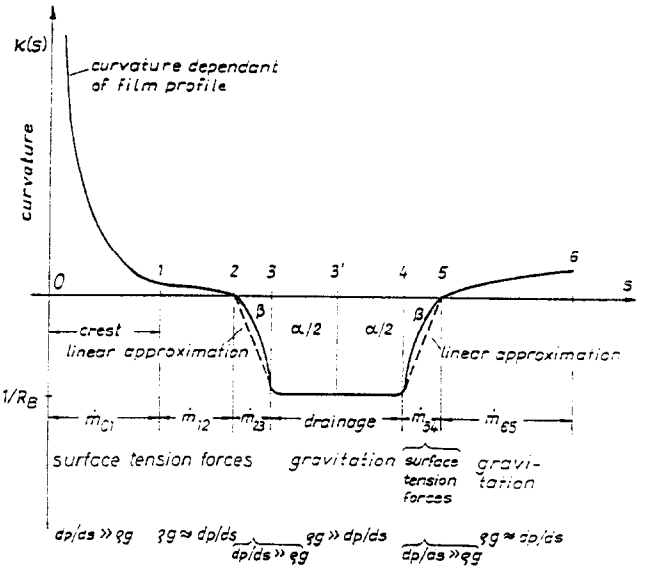

FIG. 4. Schematic showing change of curvature of the condensate film from the fin tip to the center of the drainage channel.

Using equation (23), one calculates the condensation rate on l_{23} as

$$\dot{m}_{23} = \frac{\Delta T}{\lambda}\int_0^{l_{23}} \frac{k}{\delta_{23}(s)}\,\mathrm{d}s. \tag{23}$$

4.4.3. *Condensation on* l_{12}. We have previously noted that the curvature and the curvature change over l_{12} should be quite small. A practical assumption would be to neglect the condensation over l_{12}. However, we will include this term using an approximation proposed by Honda [16]. Based on numerical calculations, he showed that approximately

$$\sigma\cdot(\mathrm{d}\kappa/\mathrm{d}s)_{12} \simeq 0.1\sigma\cdot(\mathrm{d}k/\mathrm{d}s)_{23}. \tag{24}$$

The authors have found that changing the constant 0.1 in equation (23) from 0.1 to 1.0 causes only a 2% change in the condensation rate on the total surface. Following the same procedure used above, one finds that

$$\delta_{12}(s) = \left(\left(\frac{3v\dot{m}_{01}10l_{12}R}{\sigma}\right)^{4/3} + F_{\mathrm{p}}\left(\frac{10l_{12}R}{\sigma}\right)s\right)^{1.4} \tag{25}$$

and

$$\dot{m}_{12} = \frac{\Delta T}{\lambda}\int_0^{l_{12}} \frac{k}{\delta_{12}(s)}\,\mathrm{d}s \tag{26}$$

where

$$l_{12}(z) = H-(l_{23}(z)+R^*(z)+\Delta(z)). \tag{27}$$

4.4.4. *Commentary on the model.* As previously noted, the model assumes that gravity force is negligible, compared to the surface tension force. If this is not satisfied, the actual flow field will be influenced by gravity force; thus, the flow will have velocity components in the x- and z-directions. Adamek [8] has analyzed the influence of a combined surface tension–gravity force field on flow of the condensate film. He showed that the calculated film thickness in the x-direction is nearly independent of the force in the z-direction. This means that the real film velocity may have a z-component, but the condensation rate is nearly the same as that calculated neglecting the gravity force. The approximation used here greatly simplifies the analysis.

4.5. *Condensation at the channel base surface*

4.5.1. *Specification of condensation regions.* As shown in Fig. 3, the width of the base channel, $D/2$, is made up of three incremental lengths

$$D/2 = R^*(z)+l_{54}(z)+l_{65}(z). \tag{28}$$

The condensation rate on length R^* is assumed to be zero. As shown by Fig. 1, we assume that l_{65} is drained by gravity, rather than by surface tension. It is possible that surface tension also contributes to the drainage of l_{65}, although our model does not account for this possibility. The analysis in the Appendix shows that $l_{54} \simeq l_{23}$, because of the symmetry of the circular interface in the corner of the channel. Hence, l_{54} is given by equation (20). Substitution of equation (20) in equation (28) defines l_{65}. A more precise formulation for l_{54} is given in the Appendix.

4.5.2. *Condensation on* l_{54}. Calculation of the film thickness in l_{54} parallels the procedure applied to l_{23}. However, the analysis is simpler, because none of the condensate generated in l_{65} enters l_{54}. Assuming a linear pressure gradient in l_{54}, and using equation (15), we obtain

$$\sigma\kappa'_{54} = \frac{\sigma}{l_{54}R}. \tag{29}$$

Defining the coordinate s, with $0 < s < l_{54}$ and using equation (29) in equation (13), we obtain for δ_{54}

$$\delta_{54}(s) = \left(F_p \frac{l_{54} R}{\sigma} s\right)^{1/4}. \quad (30)$$

The condensation rate on l_{54} is obtained by integrating equation (30)

$$\dot{m}_{54} = \frac{\Delta T}{\lambda} \int_0^{l_{54}} \frac{k}{\delta_{54}(s)} \mathrm{d}s. \quad (31)$$

4.5.3. *Condensation on l_{65}.* The model assumes that region l_{65} is gravity drained. Hence, the Nusselt equation (equation (13)) directly applies. Applying equation (13) to l_{65} gives

$$\delta_{65}(z) = \left(\frac{F_p}{\rho g} z\right)^{1/4}. \quad (32)$$

The resulting condensation rate on l_{65} is

$$\dot{m}_{65}(z) = \frac{\Delta T l_{65}}{\lambda} \frac{k}{\delta_{65}(z)} \quad (33)$$

where l_{65} is obtained from

$$l_{65}(z) = \frac{D}{2} - R^*(z) - l_{54}(z). \quad (34)$$

4.6. *Iterative calculation procedure*

Recall that the value of $R(z)$ was initially estimated assuming that all of the condensate was generated on l_{01}. Having developed models for the condensation rate in the channel, one may update the calculation for $R(z)$ using equation (18) with $\dot{m}_{65}(z) = 0$. $\dot{m}_{65}(z) = 0$ because the model assumes that this condensate is gravity drained, and does not enter the corner region. The proposed iterative method is easily performed using a digital computer program.

4.7. *Integration over the plate length*

The radius of the condensate film in the corner, $R(z)$, changes with length along the plate length. It is zero at the top of the plate and attains its maximum value at the bottom of the plate. Hence, the terms l_{ik} and $\dot{m}_{ik}$ also are functions of z. The total condensation rate on a plate of length L is given by equation (11).

The integration over z is easily accomplished using an incremental computation procedure in a computer program. The plate of length L is divided into N increments of length Δz over its length. Hence, $z_j = j \cdot \Delta z$, where $j = 1, 2, \ldots, N$. The values of $R(z_j)$, $l_{ik}(z_j)$ and $\dot{m}_{ik}(z_j)$ are used for calculations in the $(j+1)$th z-increment. The total condensation rate is then given by

$$\dot{M}_{tot} = \dot{m}_{01} L + \sum_j [\dot{m}_{12}(\Delta z_j) + \dot{m}_{23}(\Delta z_j) + \dot{m}_{54}(\Delta z_j) + \dot{m}_{65}(\Delta z_j)] \quad (35)$$

with $0 \leqslant j \leqslant N$. Recall that $\dot{M}_{tot}$ is the condensation rate on one-half of the fin channel, as shown in Fig. 3. The total condensation rate on a plate having N fin channels is given by

$$\dot{M}_{plate} = 2N\dot{M}_{tot}. \quad (36)$$

5. MODES OF CONDENSATION IN THE CHANNEL

The condensate flow pattern in the channel changes along the plate length, as is illustrated in Fig. 2. Thus, the terms $R(z)$ and $l_{ik}(z)$ change along the plate length. The cross-sectional area of the channel depends on the channel height (H), the convex fin height ($e-H$) and the channel width (D). For small channel heights and channel spacings, some of the condensation areas (l_{ik}) may vanish. As long as $R(z) \leqslant D/2$, the condensate thickness in the channel base (Δ) is zero, and H of Fig. 3 is equal to the sum of the components

$$H = R^*(z) + l_{23}(z) + l_{12}(z). \quad (37)$$

However, when the radii (R) join at the center of the channel, the condensate depth begins to increase, and the analysis assumes that the condensation rate on the channel base is negligible. After the radii are joined at the channel center, the radius attains the value $D/2$ and remains constant until the entire fin depth and channel depth (e) are flooded. When the condensate depth is sufficient to start flooding the convex profile, the radius may have $R \geqslant D/2$. Figure 2 illustrates this when the entire channel and fin height are flooded. As Δ increases from zero, the regions l_{12} and l_{23} will decrease. When $\Delta > 0$, H is given by

$$H = R^*(z) + l_{23}(z) + l_{12}(z) + \Delta(z). \quad (38)$$

It is necessary to define the correct equations to use for the various flow patterns illustrated in Fig. 2. This is done by defining 'condensation modes', which are associated with particular flow patterns. Three modes are defined for analysis of condensation on the side wall.

Mode A

Mode A occurs near the upper part of the plate, and exists when

$$H - (R^*(z) + l_{23}(z) + \Delta(z)) \geqslant 0. \quad (39)$$

The difference of the terms on the left-hand side of equation (39) gives the length l_{12}. If equation (39) is satisfied, the calculation procedure would use equations (9), (12) and (19) along with (20)–(27) to calculate the condensation rate on the channel side.

Mode B

Mode B is initiated following Mode A and is distinguished by the condition $l_{12}(z) = 0$. Then, $l_{23}(z)$ is given by

$$l_{23}(z) = H - (R^*(z) + \Delta(z)) \quad (40)$$

rather than by equation (20), which applies to Mode A.

Mode C

This mode exists when the condensate thickness (Δ) is so thick that both l_{12} and $l_{23}(z)$ vanish. Condensation will occur only on the convex profile.

Modes D, E, and F describe conditions that affect condensation on the channal base.

Mode D

This mode exists near the upper part of the plate, when both $l_{65}(z)$ and $l_{54}(z)$ exist. Mode D exists if

$$\frac{D}{2} - (R^*(z) + l_{54}(z)) \geqslant 0. \tag{41}$$

The length $l_{65}(z)$ is given by the left-hand side of equation (41). The condensation rate on the channel base is calculated using equations (10), (19) and (20), along with equations (28)–(34).

Mode E

This mode is attained when $l_{65}(z)$ vanishes. Then equation (20) is no longer applicable for calculation of $l_{54}(z)$. Rather $l_{54}(z)$ is given by

$$l_{54}(z) = \frac{D}{2} - R^*(z). \tag{42}$$

Mode F

After both $l_{65}(z)$ and $l_{54}(z)$ have vanished, and $\Delta > 0$, the circular interfaces will have joined at the channel center (Fig. 2(d)), and the interface radius will have the value $R = D/2$. When this condition is reached the condensation rate on the channel base is negligible.

6. COMPARISON OF THEORY WITH EXPERIMENTAL RESULTS

Kedzierski and Webb [13] measured the R-11 condensation rate on vertical plates 100 mm long and 50 mm wide, which had precisely formed convex fin profiles. The electrostatic machining method (EDM) was used to form the fin profiles, which very precisely forms the required geometry. Figure 5 shows the fin geometry formed on the plates. The total fin height consists of the convex fin profile (l_{01}), plus the channel of depth H. Two convex profile geometries were made, whose shape is defined by equation (12). The first had $\xi = 2.0$ (the Gregorig profile) and -0.5 (the Adamek profile). Three finned plates were made for each ξ-profile. They differed in the height of the drainage channel, H, as shown by Fig. 5. All of the plates had a drainage channel width of $D = 1.0$ mm. The $\xi = 2$ plate had 30 fins and the $\xi = -0.5$ plate had 36 fins, both with $l_{01} = 0.762$ mm. The objective of the tests was to determine if the experimental values for condensation on the convex profiles agreed with the theoretical values. Because the measured condensation rate includes that on both the convex profile (l_{01}) and the drainage channel of depth H and width D, it was necessary to determine the fraction of the total condensation rate which occurred on the convex profile. This was done using a modified 'Wilson plot method', as described by Kedzierski and Webb [13]. This method separated the condensation rate on the convex profile (Q_c), the sides of the channel (Q_s) and the channel base (Q_b). Thus, the total condensation rate is the sum of the components

$$Q_{tot} = Q_c + Q_s + Q_b. \tag{43}$$

We have used the present theory to predict the condensation rate, and then compare the predictions with the Kedzierski and Webb [13] data. The solid lines in Fig. 6(a) show the predicted heat transfer coefficient for all of the data taken on plates shown in Fig. 5. The dashed lines (a and g) show the predicted condensation coefficient on the convex profile only (excluding the channel). The data points are shown by the symbols. This figure shows excellent agreement between the present theory and the experimental results.

Figure 6(b) shows the predicted results on the Fig. 5 plates for $\Delta T = 5$ K. This figures shows the contributions of the three terms in equation (43). The symbol points in Fig. 6(b) show the experimental values of Q_{tot} for the plates. Lines a and c show the predicted values of Q_{tot} for the $\xi = -0.5$ and 2.0 plates, respectively. Curves b and d of Fig. 6(b) show the predicted values for the convex profiles (l_{01} in Fig. 5) for 100% fin efficiency. Thus the difference between curves a and b is the condensation rate in the channel region for the $\xi = -0.5$ surface. Similarly, the difference between curves c and d is the condensation rate in the channel region for the $\xi = 2$ geometry. Curve e (at the bottom of Fig. 6(b)) shows the condensation rate on the channel side (dimension H), and curve f shows the condensation rate on the channel base (dimension D).

The predicted values deviate from the experimental values for the $\xi = -0.5$ plates by 1, 2 and 0% for plates having H of 0.254, 0.508 and 0.762 mm, respectively. For the $\xi = 2$ plates, the predicted values deviate from the experimental values by 1, 11 and 5% for plates having H of 0.254, 0.508 and 0.762 mm, respectively. We conclude that the present theory does an excellent job of predicting the experimental values.

Figure 7 shows the percentage of the total condensation rate in the channel (Q_s and Q_b) for the $\xi = 2$ profile, as a function of the channel dimension H (see Fig. 5). Predictions are given for R-11, which was used by Kedzierski and Webb [13], and for two other fluids (R-12 and water). Figure 7 shows that the condensation rate on the channel side (Q_s) decreases rapidly as H is decreased from the highest value of 0.762 mm. Figure 8 shows the reason for this. Figure 8 shows how the terms R, l_{65} and l_{54} change with the drainage length, z. The value of R will increase along the plate length until its maximum value is attained. The maximum value of R is $D/2$, which is 0.5 mm for all of the plates. The figure shows that $R(z) > 0.25$ mm after only 1/40th of the plate length. Therefore,

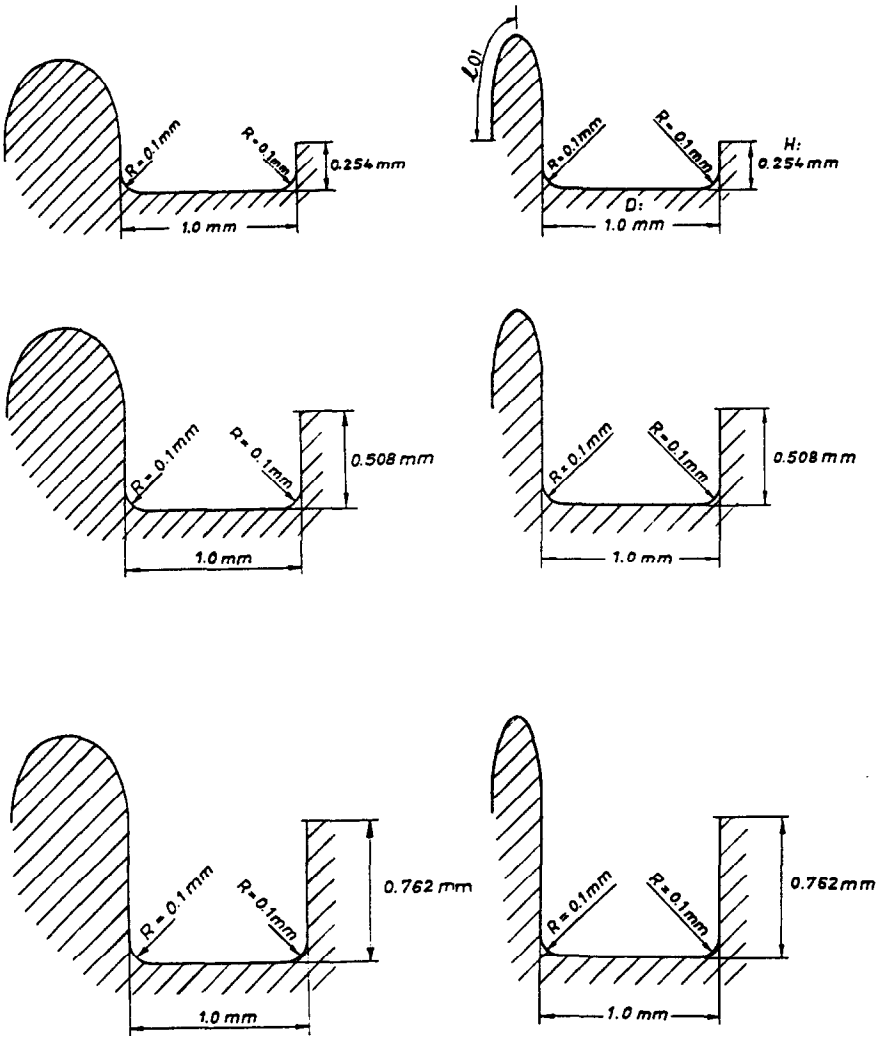

FIG. 5. Cross-section illustrations of the $\xi = -0.5$ and 2 profile plates tested by Kedzierski and Webb [13].

for the $H = 0.25$ mm channels, $Q_s = 0$ after only $z = 0.0025$ m (1/40th of the plate length). For $H = 0.5$ mm, Fig. 8 shows that $R(z) = 0.5$ mm at $z = 0.025$ m. Hence, after $z = 0.025$ m no more condensation occurs on the channel side for $H = 0.5$ mm. For $H = 0.762$ mm, the condensate radius (R) reaches its maximum value (0.5 mm) at $z = 0.025$ m, and does not change thereafter. Thus, condensation occurs on the side channel for the full length of the plate. The A-mode governs the condensation on the channel side for the $H = 0.762$ profiles. However, the C-mode governs the plates having $H = 0.25$ and 0.5 mm.

Ideally, one would choose a drainage channel dimension $H \times D$, such that $R \leqslant H$ along the entire plate length. Otherwise, the condensate film in the drainage channel will begin to interfere with the condensation process on the convex profile (l_{01}). The ideal drainage channel will allow attainment of $l_{23} = 0$ at the end of the plate length. Conversely, there is little advantage in making dimension H of the drainage channel so high that it does not completely fill to depth H. The authors plan to offer an additional publication on design of the optimum drainage channel.

The plates tested by Kedzierski and Webb [13] were

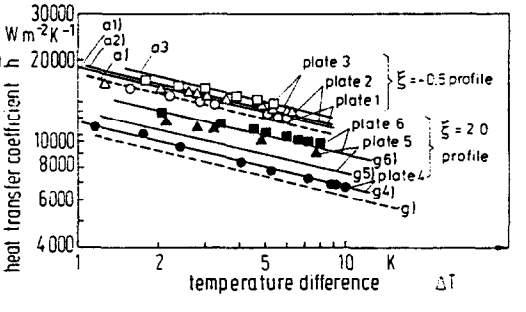

FIG. 6(a). Predicted and measured condensing coefficients on the Fig. 5 plates. (a) Line a: for $\xi = -0.5$ convex profile only. (b) Lines a1–a3: for $\xi = -0.5$ profile and channel. (c) Line g: for $\xi = 2$ convex profile only. (d) Lines g4–g6: for $\xi = 2$ profile and channel.

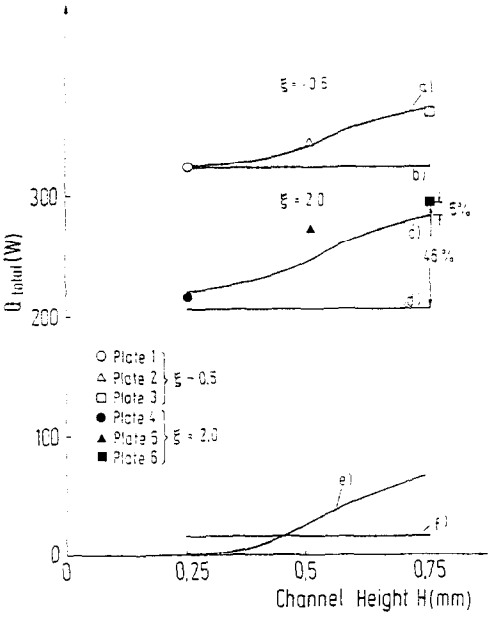

FIG. 6(b). Data and predictions for Kedzierski and Webb [13] R-11 condensation data at $\Delta T = 5$ K on the Fig. 5 plates. (a) Prediction of Q_{tot} for $\xi = -0.5$ plates. (b) Prediction of Q_c for the $\xi = -0.5$ fin profile. (c) Prediction of Q_{tot} for the $\xi = 2$ plates. (d) Prediction of Q_c for the $\xi = 2$ fin profile. (e) Prediction of Q_s. (f) Prediction of Q_b.

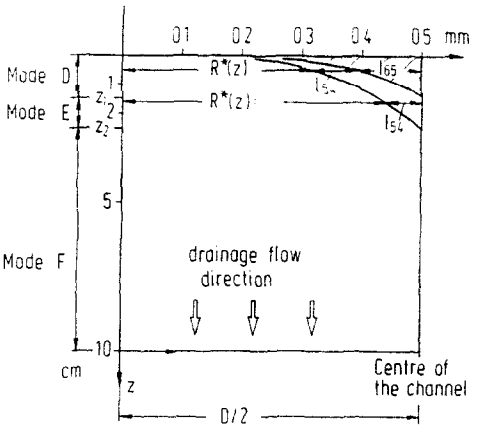

FIG. 8. Graph showing the change of R^* with distance (z) from the top of the plate. z_1 denotes where $l_{54} = 0$, z_2 denotes where $l_{65} = 0$. $R^* = D/2$ for $z \geq 2.5$ mm.

made of copper, which has high thermal conductivity ($k = 386$ W m^{-1} K^{-1}). The above analysis and discussion assumed 100% fin efficiency. We have recalculated the results using the method developed by Adamek and Webb [14] to account for the effect of fin efficiency (η_f). The $\xi = 2$ fins were quite thick (0.716 mm) and have a higher fin efficiency than the $\xi = -0.5$ profiles (0.325 mm fin thickness). The analysis showed that the fin efficiencies of the $\xi = 2$ and -0.5 plates were 0.98 and 0.94–0.96, respectively. Hence, inclusion of fin efficiency effects would produce very small results for the Kedzierski and Webb data.

The present model assumes laminar films in the gravity drained region. If the plate is quite long, it is possible that a turbulent film may exist in the gravity drained region of the channel. However, one would never expect a turbulent film in the surface tension drained regions. If the gravity drained channel were turbulent, the present analysis would tend to underpredict the total condensation rate.

7. OTHER DRAINAGE CHANNEL SHAPES

The present analysis may be easily adapted to other drainage channel shapes, e.g. the cosine shape illus-

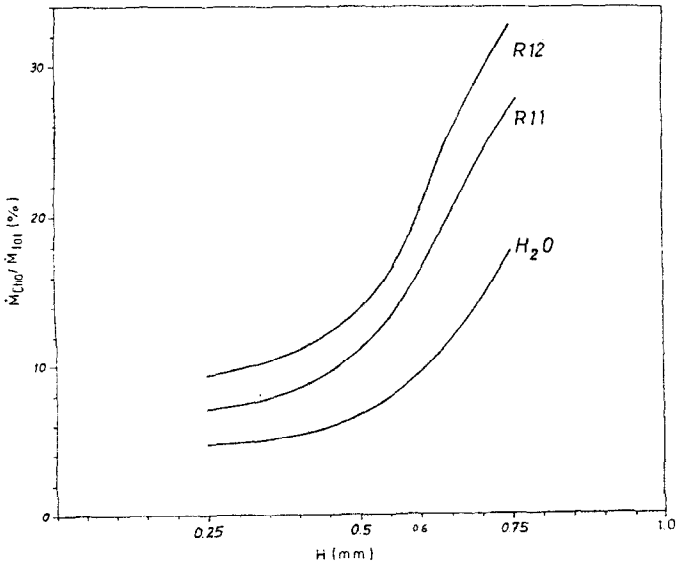

FIG. 7. Prediction of $\dot{M}_{Cha}/\dot{M}_{tot}(\%)$ for three different fluids condensing on the finned plates of Fig. 5 ($\xi = 2$).

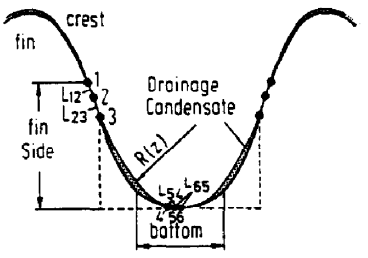

FIG. 9. Illustration of a drainage channel having a cosine cross-sectional shape.

trated in Fig. 9. The present analysis for the rectangular channel cross-section showed that less than 5% of the total condensation occurred on the channel base. For the cosine shape, we would neglect the condensation rate in the base small region (l_{54} and l_{65}) and include the contributions for l_{12} and l_{23}. Between points 3 and 4 of Fig. 9, we propose to use the present analysis for the flat side wall.

8. CONCLUSIONS

(1) A theoretical model has been developed to predict the condensation rate on the drainage channel of a vertical plate (or tube) having surface tension drained fins.

(2) Although the model was applied to channels of rectangular cross-section, it may be easily adapted to other drainage channel shapes.

(3) The theoretical model was shown to provide excellent predictions of R-11 data by Kedzierski and Webb [13].

REFERENCES

1. R. Gregorig, Hautkondensation an feingewellten Oberflächen bei Berücksichtigung der Oberflächenspannung, *Z. Angew. Math. Phys.* **5**, 36–49 (1954).
2. V. A. Karkhu, Film condensation of vapour on horizontal corrugated tube, *J. Engng Phys.* **4**, 1229–1234 (1970).
3. C. Zener and A. Lavi, Drainage systems for condensation, *J. Engng Pwr* **96**, 209–215 (1974).
4. R. L. Webb, A generalized procedure for the design and optimization of fluted Gregorig condensing surfaces, *J. Heat Transfer* **101**, 335–339 (1979).
5. T. Fujii and H. Honda, Laminar filmwise condensation on a vertical single fluted plate, *6th Int. Heat Transfer Conf.*, Toronto, Vol. 2, pp. 419–424 (1978).
6. Y. Mori, K. Hijiikara, S. Hirasawa and W. Nakayama, Optimized performance of condensers with outside condensing surfaces, *Condensation Heat Transfer*, ASME (1979).
7. C. B. Panchal and K. J. Bell, Analysis of a Nusselt type condensation on a vertical fluted surface, *Numer. Heat Transfer* **3**, 357–371 (1980).
8. T. Adamek, Bestimmung der Kondensationsgrössen auf feingewellten Oberflächen zur Auslegung optimaler Wandprofile, *Wärme- und Stoffübertr.* **15**, 255–270 (1981).
9. T. Adamek, Filmkondensation an gewellten und an eng berippten Rohroberflächen, *Chemie-Ingr-Tech.* **55**, No. 9 (1983).
10. R. L. Webb, S. T. Keswani and T. M. Rudy, Investigation of surface tension and gravity effects in film condensation, *7th Int. Heat Transfer Conf.*, Munich, Vol. 5, pp. 175–181 (1982).
11. R. L. Webb and T. M. Rudy, An analytical model to predict condensate retention on horizontal, integral fin tubes, *J. Heat Transfer* **107**, 361–366 (1985).
12. H. Honda and S. Nozu, A prediction method for heat transfer during film condensation on horizontal low integral-fin tubes, *J. Heat Transfer* **108**, 218–225 (1986).
13. M. A. Kedzierski and R. L. Webb, Experimental measurements of condensation on vertical plates with enhanced fins, *Boiling and Condensation in Heat Transfer Equipment*, ASME Symp. Vol. 87—HTD/ Vol. 85, pp. 87–95 (1987).
14. T. Adamek and R. L. Webb, Prediction of film condensation on horizontal integral fin tubes, *Int. J. Heat Mass Transfer* **33**, 1721–1735 (1990).
15. D. G. Thomas, Enhancement of film condensation rate on vertical tubes by longitudinal wires, *A.I.Ch.E. Jl* **14**, 644–649 (1968).
16. H. Honda, A prediction method for heat transfer during film condensation on horizontal low integral fin tubes, *ASME HTD* **38**, 107–114 (1984).

APPENDIX. CALCULATION OF l_{23}, l_{54} and R^*

High heat transfer coefficients can exist in thin film regions l_{23} and l_{54} of Fig. 3. These thin film regions can occur near the upper part of the plate if the channel dimensions H and D are sufficiently large. Figure 3 shows that film regions l_{23} and l_{54} exist at symmetric locations about the corner of the drainge channel. The surface tension pressure gradient over l_{23} is given by equation (16). The same equation applies to l_{54} (replace subscript '23' by '54'). However, there is a significant difference in the film flow rate at regions l_{23} and l_{54}. Section l_{23} is subjected to a strong mass flow m_{02}, which enters the section at point 2, while the mass flow into the section l_{54} is negligible. As illustrated in Fig. 1, we will assume that the condensate flow m_{65} is governed by gravitation only, and hence will not cross the boundary l_{54}.

Calculation of l_{54}

The film flow in region l_{54} is surface tension driven by the change of the interface curvature from a linear to a circular form (Figs. 3 and 4). Between points 3 and 4, the curvature of the interface is $-1/R(z)$, with radius $R(z)$ depending on the drainage flow rate. Since $R(z) \leqslant s/2$, the pressure at point 4, $-\sigma/R(z)$, is very low compared to the pressure at point 5, which has zero curvature ($r = \infty$). Hence, a strong pressure gradient exists over l_{54}, which pulls the condensate toward the fin base. Our model assumes that the pressure gradient over l_{54} is linear (Fig. 4). The rotation angle β traversed over l_{54} is given by the integral of the curvature over l_{54}. This integral is the area under the triangle for region l_{54} of Fig. 4, which assumes a linear curvature change. So, in mathematical terms we may write

$$l_{54} = 2R\int_{x=4}^{x=5} \kappa(x)\,dx = 2R\beta. \qquad \text{(A1)}$$

Unfortunately, the magnitude of the angle β is not known, although we expect it to be a small angle, e.g. 10–15°. We will determine β by writing two independent equations for the film thickness at point 4 of Fig. 3, each of which will contain l_{54} and β. Figure 3 shows that R^* is the projection of R onto the fin at point 4. Using the cosine relationship and $\delta_{54} = R - R^*$, we write $\delta_{54}/R = 1 - \cos\beta$. Substituting $\beta = \delta_{54}/2R$ from equation (A1), we obtain

$$\delta_{54} = R(1-\cos\beta) = R\left(1-\cos\left(\frac{l_{54}}{2R}\right)\right). \qquad \text{(A2)}$$

To obtain the second equation, we will assume a linear

surface tension pressure gradient over l_{34}. The condensate film thickness associated with this assumption is obtained using the Nusselt equation (equation (13)) with equations (14) and (15). Thus, we replace ρg in equation (13) by $\sigma/l_{54}R$ and z by l_{54}. The film thickness at point 4 ($x = l_{54}$) is thus given by

$$\delta_{54} = [F_p l_{54}^2 R/\sigma]^{1/4}. \quad \text{(A3)}$$

Equation (A3) assumes that no condensate flows from region l_{56} into region l_{54}. Substitution of equation (A2) in (A3) gives

$$R[1-\cos(l_{54}/2R)] = (F_p R l_{54}^2/\sigma). \quad \text{(A4)}$$

Although equation (A4) may be iteratively solved for l_{54}, sufficient accuracy will exist by expanding the cosine term into a Taylor series, and using the first two terms of the series. The resulting approximation for l_{54} is

$$l_{54} = [F_p R^5/\sigma]^{5/6}. \quad \text{(A5)}$$

Application of equation (A5) to practical condensation problems yields reasonable results for β. For example, condensation of R-11 at 1 atm in a channel having $R = 0.4$ mm yields $\beta = 10^\circ$.

Calculation of l_{23} and δ_{23}

Because of the symmetry of the drainage channel, the simplest assumption is to set $l_{23} = l_{54}$. However, this approximation will slightly underpredict l_{23}, because it does not account for the condensate entering at point 2. Recall that no condensate entered point 5 for the calculation of l_{54}. A more precise estimate of l_{23} is obtained by accounting for the condensate entering at point 2. The local film thickness in a surface tension drained region is given by Adamek [8] as

$$\delta^4(x) = (F_p/\sigma)(\kappa')^{-4/3}\int_0^x (\kappa')^{1/3}\,dx. \quad \text{(A6)}$$

Equation (A6) is to be integrated over regions l_{12} and l_{23}, which are bounded by $x_1 \leqslant x \leqslant x_3$. The curvature gradient, κ', is constant over these regions, and is equal to f_{12}/σ and f_{23}/σ for regions l_{12} and l_{23}, respectively. Substitution of these values in equation (A6) and writing the integral over the two regions gives for $\delta_{23}(x)$

$$\delta_{23}(x) = \left[\delta_{01}(f_{12}/f_{23})^{-4/3} + \int_0^t (f_{12}/\sigma)^{-1/3}\,dt\right]^{-1/4} \quad \text{(A7)}$$

where $t = x - x_1$. Solution of the momentum equation for the average condensate velocity and use of the continuity equation gives the mass flow rate

$$\dot{m}_{12} = f_{12}(\delta_{12})^3/3\nu \quad \text{(A8)}$$

and at $x = x_1$, conservation of mass requires

$$f_{12}(\delta_{12})^3 = f_{23}(\delta_{23})^3. \quad \text{(A9)}$$

Substitution of equations (A8) and (A9) in equation (A7), along with $f_{23} = \sigma/Rl_{23}$, gives the final result

$$\delta_{23}(x) = [(3\nu\dot{m}_{02}Rl_{23}/\sigma)^{4/3} + F_p R l_{23} x/\sigma]^{1/4}. \quad \text{(A10)}$$

The term $\dot{m}_{02}$ is the condensate rate crossing point 2 in Fig. 3. An iterative solution of equation (A10) is required since it may not be explicitly solved for l_{23}, and because $\dot{m}_{02} = \dot{m}_{01} + \dot{m}_{12}$ is not known. Since we expect $\dot{m}_{12} \ll \dot{m}_{01}$ a reasonable approximation is to use $\dot{m}_{02} \simeq \dot{m}_{01}$.

If the approximation $l_{23} = l_{54}$ is used, the channel condensation rate ($\dot{M}_{Cha}$) may be underpredicted by approximately 2%, which would result in significantly less than 1% error in $\dot{M}_{tot}$. Hence, the complication associated with equation (A10) may not be warranted.

Calculation of R^*

The relation between R and R^* is obtained from Fig. 3. Using the definition $\alpha = \pi/4 - \beta$, we obtain

$$R^*(z) = R(z)\cdot\cos\alpha = R(z)\cdot\cos(\pi/4-\alpha)$$
$$= R(z)\cdot\cos[l_{23}(z)/2R(z)]. \quad \text{(A11)}$$

PREDICTION DE LA CONDENSATION EN FILM SUR DES PLAQUES ET DES TUBES AILETES: UN MODELE POUR LE CANAL DE DRAINAGE

Résumé—En 1954 Gregorig a formulé une théorie pour la condensation drainée par tension superficielle sur des surfaces striées verticales. De telles surfaces peuvent avoir un canal de drainage dans lequel le condensat formé sur un profil convexe spécial est drainé par gravité. On trouve des écrits qui veulent formuler un modèle satisfaisant pour prédire la condensation dans le canal de drainage. On formule ici une méthode théorique pour prédire la condensation dans un canal de drainage à section droite rectangulaire. Le modèle est utilisé pour décrire les expériences de Kedzierski et Webb, et on obtient une bonne prédiction des données expérimentales. Le débit de condensat dans le canal de drainage compte pour 6 à 32% du débit total obtenu avec le profil d'ailette convexe de Gregorig, comme vérifié par Kedzierski et Webb. Avec une légère modification, le modèle peut être étendu pour prédire le débit de condensat dans des canaux ayant une forme autre que rectangulaire, par exemple une forme sinusoïdale.

BERECHNUNG DER FILMKONDENSATION AN SENKRECHTEN BERIPPTEN PLATTEN UND ROHREN—EIN MODELL FÜR DEN ABFLUSSKANAL

Zusammenfassung—Im Jahre 1954 formulierte Gregorig eine Theorie für die Kondensation an senkrechten, speziell strukturierten Oberflächen mit konvexen Rippenprofilen. Von diesen Oberflächen fließt das Kondensat infolge der Oberflächenspannung ab. Typischerweise müssen diese Oberflächen einen Abflußkanal besitzen, in dem das auf den speziellen konvexen Profilen gebildete Kondensat durch die Schwerkraft abfließt. In der Literatur befindet sich bisher kein befriedigendes Modell, das die Berechnung der Kondensationsrate im Abflußkanal erlaubt. In dieser Arbeit wird eine theoretische Methode erläutert, die die Berechnung der Kondensationsrate in einem Abflußkanal mit rechteckigem Querschnitt erlaubt. Das Modell wird benutzt, um die experimentellen Daten von Kedzierski und Webb nachzurechnen, wobei sich eine exzellente Übereinstimmung zeigt. Die Berechnung ergibt, wie auch von Kedzierski und Webb gemessen, daß die Kondensationsrate im Abflußkanal 6–32% der gesamten Kondensationsrate an konvexen Grigorig-Rippenprofilen beträgt. Das Modell für den Abflußkanal kann mit leichten Modifikationen zur Berechnung der Kondensationsrate in Abflußkanälen anderen Querschnitts, z. B. sinusförmige Querschnitte, ausgedehnt werden.

ПЛЕНОЧНАЯ КОНДЕНСАЦИЯ НА ВЕРТИКАЛЬНЫХ ОРЕБРЕННЫХ ПЛАСТИНАХ И ТРУБАХ: МОДЕЛЬ ДРЕНАЖНОГО КАНАЛА

Аннотация—В 1954 г. Грегориг сформулировал теорию конденсации с учетом поверхностного натяжения и стока на вертикальных "гофрированных" поверхностях с особым выпулым профилем ребер. Как правило, такие гофрированные поверхности имеют дренажный канал, по которому образующийся на выпуклом профиле конденсат отводится под действием силы тяжести. До сих пор в литературе отсутствовала удовлетворительная модель для определения скорости конденсации в дренажном канале. В данной статье сформулирован теоретический метод расчета скорости конденсации в дренажном канале прямоугольного сечения. С использованием предложенной модели получены теоретически экспериментальные данные Кедзерского и Вебба, и обнаружено хорошее согласие расчетов с экспериментом. Расчет показал, что скорость конденсации в дренажном канале составляет 6–32% от общей ее скорости на ребрах выпуклого профиля, предложенного Грегоригом, что также подтверждено Кедзерским и Веббом. После небольших модификаций данная модель дренажного канала может применяться для определения скорости конденсации в каналах другой, например, косинусоидальной формы.